A MAXWELL-ELASTO-BRITTLE RHEOLOGY FOR SEA ICE MODELING

By Véronique Dansereau[1], Jérôme Weiss[2], Pierre Saramito[3], Philippe Lattes[4] and Edmond Coche[5]

[1] LGGE, CNRS UMR 5183, Université de Grenoble, Grenoble, France
[2] ISTerre, CNRS UMR 5275, Université de Grenoble, Grenoble, France
[3] LJK, CNRS UMR 5224, Université de Grenoble, Grenoble, France
[4] TOTAL S.A. - DGEP/DEV/TEC/GEO, Paris, France
[5] TOTAL S.A. - DGEP, Paris, France

Abstract

A new dynamical model, which builds on the recent elasto-brittle (EB) rheology, is developed in the context of the operational modeling of sea ice conditions over the Arctic. The EB model is modified by adding a viscous relaxation term to the linear-elastic constitutive relationship together with an ''apparent'' viscosity that evolves according to the local thickness, concentration and damage of the ice, like its elastic modulus. The coupling between the level of damage and both mechanical parameters is such that within an undamaged ice cover, the viscosity is infinitely large and deformations are strictly elastic, while along highly damaged zones, such as opening leads, the elastic modulus vanishes and most of the stress is dissipated through permanent deformations. In this augmented EB model, named Maxwell-EB after the Maxwell rheology, the irreversible and recoverable deformations are solved for simultaneously, hence ice drift velocities are defined naturally. Early idealized simulations, without advection but in which the ice is allowed to damage and heal, show the model is able to reproduce the strong heterogeneity and intermittency and the anisotropy that characterize the deformation of sea ice.

Introduction

A proper representation of the mechanical behavior of sea ice is essential for making reliable predictions of ice conditions and drift, especially over the fine scales involved in operational modeling. In recent years, statistical analysis of available ice buoy drift and Radarsat Geophysical Processor System (RGPS) drift data have revealed the strong heterogeneity and intermittency of Arctic ice deformation (Marsan et al., 2004; Rampal et al., 2008), suggesting that the deformation of the pack is mostly accommodated by elastic interactions and brittle fracturing over a wide range of scales. Current operational modeling platforms (e.g., TOPAZ4 : Sakov et al., 2012, Canadian Global Ice Ocean Prediction System : Smith et al.. 2014) and coupled climate models, some with and some without data assimilation, are based on the same viscous-plastic (VP) rheological framework put forth in the late seventies (Hibler, 1977; 1979). Yet, this rheology is inconsistent with the observed elasto-brittle behavior of pack ice (Weiss et al., 2007) and recent studies have demonstrated that although it can represent with a certain level of accuracy the mean, global (> 100 km) sea ice drift, it effectively fails at reproducing the right amount and the characteristics of sea ice deformation, especially at small (regional, daily) scales (Girard et al., 2009).

Over the last few years, a new rheological framework named ''elasto-brittle" (EB) has been developed as an alternative to the VP rheology for continuum sea ice models, in which the ice cover is treated as a two-dimensional, isotropic, elastic, damageable material (Girard et al., 2011). The model combines:

- A linear elastic constitutive relationship for a continuum solid under plane stress,

$$\sigma = E\varepsilon(U), \qquad (1)$$

with $\boldsymbol{\sigma}$, the stress tensor, $\boldsymbol{\varepsilon}$, the strain tensor (in terms of the displacement, $\boldsymbol{U}$) and E, the elastic modulus of sea ice.

- A Mohr-Coulomb criterion for brittle failure, in agreement with in-situ stress measurements (Weiss et al., 2007),

$$\tau = \mu\sigma_N + C, \qquad (2)$$

With $\boldsymbol{\tau}$ and $\boldsymbol{\sigma_N}$, the shear and normal stresses, C, the cohesion, setting the resistance to pure shear and μ, the internal friction coefficient, set to the value of 0.7 commonly used for geo-materials and ice (Byerlee, 1978; Jaeger and Cook, 1979; Weiss and Schulson, 2009). In the model, a noise is introduced in the spatial distribution of the ice strength through the cohesion parameter C to represent the material's natural heterogeneity associated with structural defects at the sub-grid scale, such as thermal cracks, serving as stress concentrators. The randomly drawn values of C span estimates from in-situ stress measurements in Arctic sea ice (Weiss et al., 2007).

- A progressive isotropic damage mechanism for the elastic modulus representing fracturing and lead formation within the pack. By this process, *E* drops when the stress state locally exceeds the Coulomb failure envelope, resulting in local strain weakening or "damaging". Consistent with previous damage rheological models, the level of damage of the sea ice cover in the EB framework is represented by a non-dimensional, scalar parameter, *d*, evolving between 0 ("completely damaged") and 1 (undamaged pack) and interpreted as a measure of defects (crack) density (Kemeny and Cook, 1986). Because of the long-range interactions in the elastic medium, local drops in *E* associated with the damaging of model elements imply a stress redistribution that can in turn induce damage of neighboring elements. By this process, damage therefore propagates within the pack.

First implementations of this rheology into short (3-days), stand-alone realistic simulations of the Arctic ice pack forced with reanalysis winds and *without advection* showed the EB model is able to reproduce the strong localization and the anisotropy of damage and agrees very well with the deformation fields estimated from RGPS data (Girard et al., 2011). In the context of longer-term simulations of ice conditions, over which advective processes can no longer be neglected, a suitable dynamical ice model however needs to represent not only the small deformations associated with

the fracturing of the elastic ice pack, but also the larger, permanent deformations occurring once the pack is fragmented and undamaged plates move relative to each other along open leads, setting the overall drift pattern and velocity of the ice, ***u***. The goal of this work is to develop such a rheological framework allowing a passage between small and large deformations while retaining the capacity of the EB model to reproduce the observed anisotropy and scaling properties of sea ice.

The Maxwell-EB model

Estimating unambiguously the ice velocity field over days and longer time periods requires distinguishing between the elastic (reversible) and the permanent (irreversible) deformations occurring once the pack is damaged. This is an intrinsic limitation of the EB rheology, since the linear-elastic model solves for the total deformation $(\varepsilon_{total} = \varepsilon_E + \varepsilon_P)$ of the material only. If no further assumptions are made on the part of the stress that is dissipated through permanent deformations after the onset of damaging, the EB model can effectively be used between two limit cases:

1. The first assumes that all of the deformation is elastic. If a stress is applied to the EB material during a time Δt and then removed, its deformation is entirely recovered, even if damage has occurred and the elastic modulus is degraded (see figure 1, left panels). The material returns to its initial position, and the velocity is effectively zero. For an initially undamaged, uniform material (or isolated model grid element) with elastic modulus E^0, the loading and unloading paths are represented respectively by the thick black line and dashed purple line on the stress-strain diagram of figure 2.

2. The second case makes the assumption that all the deformation becomes permanent. In this limit, the material retains its new position when the stress is removed, with the unloading path represented by the blue dashed line on figure 2, and the velocity is trivially estimated from the displacement as $u = \varepsilon_P / \Delta t$.

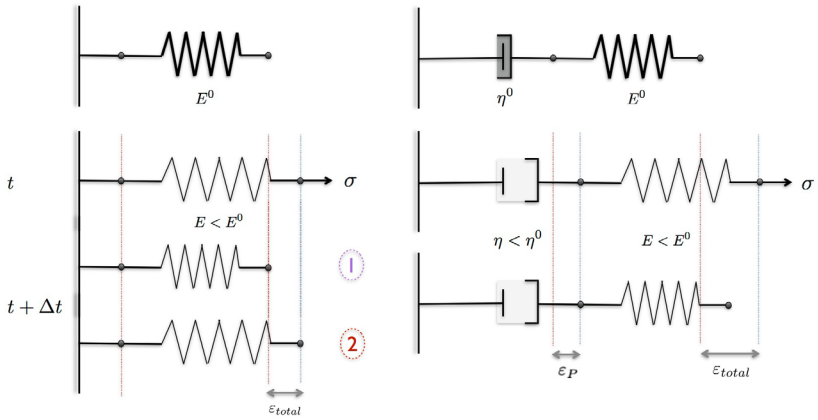

Figure 1: Schematic representations of the EB (left) and Maxwell-EB (right) models for a uniform material (or isolated model element) with initial, undamaged elastic modulus E^0 and viscosity η^0. At time t, an overcritical stress is applied on the system and is removed suddenly at time t+Δt. In the EB model, the spring deforms and weakens ($E < E^0$) when loaded. In the all-elastic deformation limit (1), it returns to its initial position when the system is unloaded. In the all-permanent deformation limit (2), it keeps its new position, and $\varepsilon_P = \varepsilon_{total}$. In the Maxwell-EB model, both the spring and dashpot deform under the applied stress such that $\varepsilon_{total} = \varepsilon_P + \varepsilon_E$, with a degradation of both E and η due to damaging. When the stress is removed, the spring returns to its initial position but the dashpot keeps its new position, resulting in a net permanent deformation, $\varepsilon_P \neq \varepsilon_{total}$.

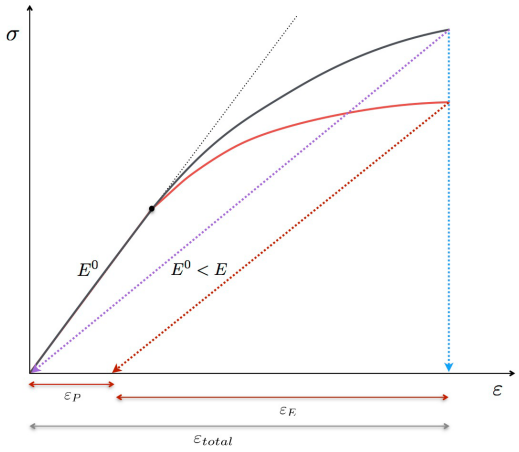

Figure 2: Stress-strain diagram for a linear-elastic (dotted curve), EB (plain black curve) and Maxwell-EB (red curve) material with initial uniform elastic modulus E^0. The black dot indicates the onset of damaging of the material. The purple and blue dashed lines represent the unloading paths for the EB material in the all-elastic and all-permanent deformation limits respectively. The red dashed curve represent the unloading path in the case of the Maxwell-EB model, with the red arrows partitioning the total deformation into the permanent and elastic contributions. It is important to note that the diagram is not to scale in the case of sea ice, in the sense that permanent deformations are usually much greater than elastic deformations.

In the case of sea ice, the second assumption might be justified by the fact that elastic deformations within an undamaged pack are small compared to the permanent deformations associated with the opening, closing, and shearing along leads. For instance, Bouillon et al. (unpublished) argued that there is a separation of 4 orders of magnitudes between the daily average deformation of a completely damaged ice pack in free drift mode and that of an undamaged, strictly elastic pack. However, in this limit, all of the stress is dissipated into permanent deformations at the end of each loading experiment, hence the *memory* of the stress associated with elastic deformations is erased after each simulated forcing increment (i.e., each model time step). Without carrying the history of previous stresses, the model cannot reproduce one important characteristic of the deformation which is its strong localization *in time*, or intermittency. In order to estimate adequate drift velocities while reproducing both the observed space and time scaling properties of sea ice deformation, a suitable rheological model must therefore have the capacity to distinguish between reversible and irreversible deformations.

In order to achieve this, we add a Newtonian fluid-like viscous damping term to the EB linear elastic constitutive equation, which then takes the form of the Maxwell rheology for continuum viscous-elastic materials:

$$\frac{1}{E}\frac{D\sigma}{Dt} + \frac{1}{\eta}\sigma = \dot{\varepsilon}(u), \qquad (3)$$

with $\dot{\varepsilon}(u)$ the strain rate. This Maxwell model is typically represented by a spring and a dashpot connected in series (see figure 1, right panels). When a stress is applied to the system, the resulting deformation is effectively split between two components: the instantaneous, reversible, deformation of the spring, $\boldsymbol{\varepsilon_E}$, and the permanent deformation of the dashpot, $\boldsymbol{\varepsilon_P}$, increasing linearly with time. For a given deformation applied to the Maxwell material $\boldsymbol{\varepsilon_{total}}$, the rate of dissipation of the associated stress through the permanent deformation of the dashpot is determined by the ratio, λ, of the viscosity of the dashpot, η, and the elastic modulus of the spring, *E*. As this characteristic relaxation time decreases, the capacity of the Maxwell material to propagate elastic constraints and retain the memory of reversible deformations also decreases. The introduction of a linear viscous term within damaged zones is justified by (i) the viscous-like rheology of highly fragmented (granular) media (Jop et al., 2006) and (ii) analogy between the mechanical behavior of sea ice and that of the lithosphere and the existence of "creeping" faults sliding aseismically within Earth's crust (Scholz, 2002).

The constitutive relationship in this modified EB model, named Maxwell-EB, differs from that of the standard Maxwell model in that the mechanical parameters *E, η* and *λ* are not constant but all coupled to the local level of damage of the material, *d*. The coupling is such that

- Undamaged areas of the ice cover undergo only small, strictly elastic deformations. These portions of the pack have an undamaged elastic modulus E^0 and an infinitely large apparent viscosity ($\eta^0 \rightarrow \infty$). In this limit, the viscous term (2nd term, LHS) in the Maxwell constitutive relationship (3) vanishes and a linear-elastic rheology is recovered.
- Over highly damaged areas of the pack, deformations are large as ice floes drift along open leads with much reduced friction. Both the elastic modulus and the apparent viscosity of the pack drop, resulting in larger instantaneous deformations that become irreversible more rapidly. Consequently, elastic interactions are inhibited and most of the stress applied to the ice cover dissipates into large, permanent deformations within a short relaxation time λ.

Different formulations can be used to couple *E, η* and *λ* in terms of *d* that respect the behavior described above. In the absence of physical evidence for a higher level of complexity, we chose the simplest parameterization and set $E = E^0 d$, $\eta = \eta^0 d^\alpha$ with $0<d \leq 1$ and α a constant parameter greater than one, introduced so that the relaxation time λ also decreases with increasing damage. As there is in theory no upper bound to this parameter, the appropriate value for α is determined through sensitivity tests. In a dynamic-thermodynamic model, E, η and λ would also be coupled to the concentration and thickness characteristics of the ice cover. In the following description of the uncoupled Maxwell-EB model, only the dependence on the level of damage is included.

In the Maxwell-EB framework, the level of damage of the ice cover evolves locally through two competing mechanisms: damaging and healing. At a given time, the decrease in *d* due to damaging is estimated as a function of the instantaneous distance of the local state of stress to the local damage criterion, $\boldsymbol{d_{crit}}$. The time, $\boldsymbol{t_d}$, associated with this change is deduced from the effective speed of propagation of elastic (shear) waves carrying the damage information within the ice cover, which is on the order of 500 m/s (Marsan et al., 2011). From current global climate to high resolution regional models, i.e., models with spatial resolution *Δx* ranging between 1 and 100 km, $\boldsymbol{t_d}$ varies between a few seconds and several minutes. The increase of d due to healing represents the re-consolidation and strengthening of the damaged ice pack due to the refreezing of open leads. This process is distinguished from pure thermodynamic growth in that it applies only where and when the ice has already been damaged. It therefore does not represent a net thickening of the ice cover and allows *d* to re-increase at *most* to its undamaged value of 1. The rate of healing is set by the characteristic time $\boldsymbol{t_h}$, corresponding to the time for a completely damaged element to regains its initial stiffness. In a coupled dynamic-thermodynamic model, $\boldsymbol{t_h}$ would depend on the difference between the temperature of the air above the ice and the freezing point of seawater below. In the present uncoupled model however, it is constant in both space and time and the rate of healing, set to $1/\boldsymbol{t_h}$, is therefore constant. Values on the order of 10^5 seconds are used for $\boldsymbol{t_h}$, based on studies on the refreezing within open leads (Petrich, 2007). Even though both processes act simultaneously on the level of damage, the orders of magnitude of difference between td and th imply that the mechanisms are intrinsically decoupled in time.

This new dynamic Maxwell-EB modeling framework for sea ice can therefore be summarized as a set of four equations:

- The momentum equation for sea ice

$$\frac{\partial u}{\partial t} + (u \cdot \nabla)u = F_{ext} + \nabla \cdot \sigma \qquad (4)$$

with the first term on the right hand side representing all external stresses on the ice and the last, the rheology term, the contribution from the mean internal stresses associated with the mechanical interactions between the ice floes,

The Maxwell constitutive relationship (3), with the elastic modulus and apparent viscosity of the ice entirely defined in terms of their initial, undamaged values and of the level of damage, *d*,

The equation of evolution for the level of damage, d, combining the rate of decrease due to damaging, set as a function of the local distance to the Mohr-Coulomb type damage criterion, and the rate of increase due to healing,

$$\frac{\partial d}{\partial t} + (u \cdot \nabla)d = f(d_{crit})\frac{1}{t_d}d + \frac{1}{t_h} \text{ with } 0 < d \leq 1. \qquad (5)$$

The advection equation for the cohesion field, C, which sets the local damage criterion,

$$\frac{\partial C}{\partial t} + (u \cdot \nabla)C = 0. \qquad (6)$$

Associated with the addition of the viscous relaxation term for the stress in the EB framework is the reformulation of the constitutive relationship in terms of the ice velocity, as opposed to the ice *displacement*, and the introduction of the time derivative of the stress tensor. The objective (Jaumann) derivative expends in three terms: an inertial term, an advection term, and rotation terms that arise because the Cauchy stress changes with rigid body rotation (rotation of the principal axes). Each of these contributions implies an increased level of numerical complexity. In developing the Maxwell-EB model, the approach taken is to introduce these terms separately and evaluate their contribution to the simulated dynamics. On the one

hand, introducing the inertial term first while neglecting advection (and rotation) allows retaining a Lagrangian scheme, similar to the EB model. If not employing adaptive remeshing methods, the model is then suitable for small-deformation simulations only. A large deformation, Eulerian, model on the other hand necessitates the inclusion of the non-linear advection term, with rotation terms becoming potentially important. In the following, first small-deformation experiments over domains with simplified geometries are analyzed in terms of the anisotropy, heterogeneity and intermittency of the simulated damage and deformation.

First simulation results: small-deformation experiments

When neglecting advection, the Maxwell-EB model reduces to three equations (3, 4, 5) for the ice velocity ***u*** (2 components), the state of stress ***σ*** (3 components), and the level of damage *d*. Time derivatives in the small-deformation model are approached with a Backward Euler scheme of order 1. A semi-implicit scheme is used to linearize the system, in which the momentum (4) and constitutive (3) equations are first solved simultaneously using the field of damage (i.e., the mechanical parameters *E, η*) at the previous time step. The level of damage is then updated using the newly estimated ***u*** and ***σ***. A fixed point algorithm iterates between these two computational steps, ensuring the convergence of the solution. The linear, time-discretized system of equations is solved using finite elements and variational methods within the C++ environment RHEOLEF (Saramito, 2013: http://cel.archives-ouvertes.fr/cel-00573970).

First simulations represent a two-dimensional, horizontal, rectangular plate of ice with height-to-width ratio of 2 under uniaxial compression (see figure 3, top left panel). The bottom edge of this sample is maintained fixed in the y-direction (with the position of the bottom left corner fixed in both directions). No confinement is applied on both lateral sides. The plate is compressed by prescribing Fext either as a small, constant increment of downward displacement (strain-controlled experiments) or force (stress-controlled experiments) on the upper boundary.

Here, two strain-driven uniaxial compression experiments are presented, the first with only the damaging mechanism operating and the second including both damaging and healing. The two simulations start with an undamaged plate with uniform elastic modulus E^0. The inverse of the viscosity η is set to zero when and where the ice is undamaged (d = 1) to represent the limit of $\boldsymbol{\eta 0} \rightarrow \infty$. The same cohesion field and unstructured mesh with triangular elements are used. The model is made completely dimensionless. The time step is set to unity, as the characteristic time for damage, $\boldsymbol{t_d}$, which ensures the highest resolution of damage propagation by the model. The characteristic time for healing is set to $\boldsymbol{t_h}$ = 10^5 seconds and a value of 4 is used for the exponent ***α***.

Figure 3 shows the macroscopic stress as a function of the applied strain throughout the damage-only simulation (black line), with numbered panels showing the field of *d* at different stages of the loading experiment. The stress-strain relationship is initially linear as the undamaged material is strictly elastic. The blue line shows the number of overcritical elements as a function of the incremental strain. After the onset of damage (black dot), the material diverges from the linear-elastic behavior and experiences some strain-softening. In the early stage of damaging, damage is homogeneously scattered over the plate (*d* panel 1). Then as the number of overcritical elements increases, damage starts to localize (panel 2). A sharp increase in overcritical elements and subsequent large drop in macroscopic stress characterize the propagation of a distinct, oriented fault, or lead, throughout the sample (panels 3 and 4). Once this feature is formed, damaging stops. The macroscopic stress stabilizes at a low value, as the imposed strain is dissipated by creep along the lead. The shear and divergent strain rate fields, strongly correlated in space, indeed show that at this point deformation rates are orders of magnitude higher along the highly damaged than over the undamaged parts of the plate (bottom right panels).

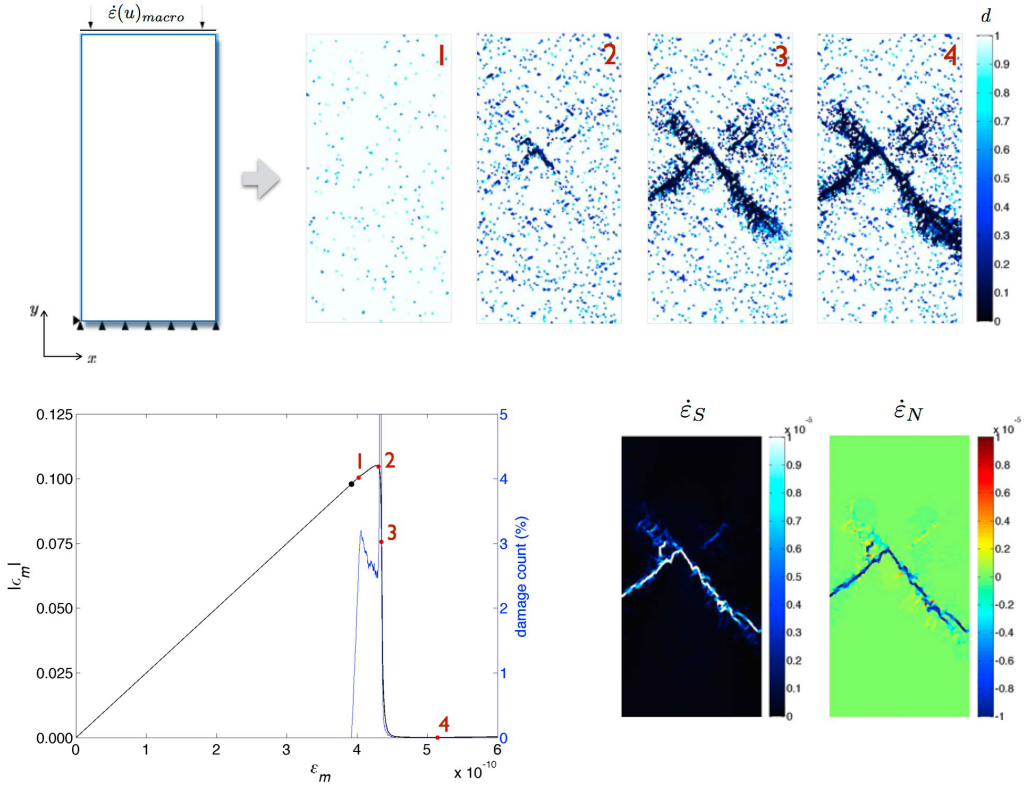

Figure 3: Results of the damaging-only uniaxial compression experiment. Top left panel: schematic representation of the boundary conditions and forcing imposed on the 2D simulated sample of ice. Bottom left panel: macroscopic stress as a function of the prescribed macroscopic strain (black curve) and corresponding percentage of overcritical model elements (blue curve). The black dot indicates the onset of damaging. Top right panels: level of damage at four stages of the experiments indicated on the stress-strain curve. Bottom right panels: shearing and divergence (positive) strain rates after the propagation of the main fault across the sample (stage 4).

When the compressive loading is maintained and the simulated material is also allowed to heal, a complex behavior emerges that is characterized by a succession of sharp stress drops associated with the localization of damage and propagation of faults and slower recovery periods during which the material regains some stiffness and stress buildups (see figure 4). These asymmetric and irregular cycles arise while the applied forcing is strictly uniform in time. Snapshots of the order of magnitude of the shearing deformation rate at different stages of the simulation (lower panels on figure 4) show that some cycles are associated with the re-activation of partially healed faults, while others are characterized by the formation of new features with different shapes and orientation, as observed in RGPS data (Kwok 2001). During stress-buildup phases, deformation increases everywhere over the sample. Stress drops abruptly when failure occurs and strain concentrates over the highly damaged areas, where it is orders of magnitude (≥3) higher than over undamaged areas. The experiment also reveals that in some instances, systems of fractures can remain activated for some time, in which case the macroscopic stress stabilizes (eg., panels 1 and 2), suggesting a balance between the rate of loading, the creeping and the rate of healing of the faults.

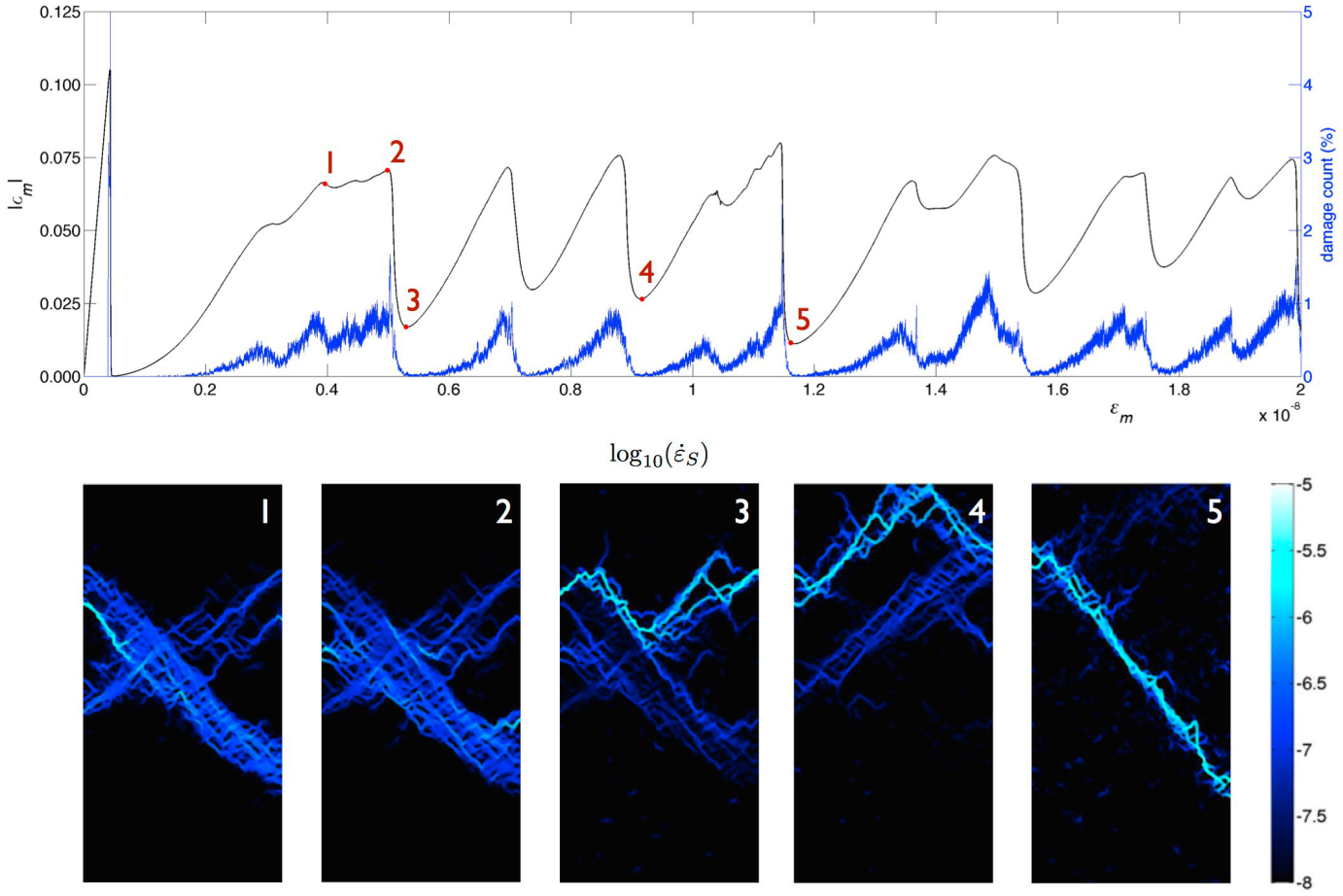

Figure 4: Results of the damaging and healing uniaxial compression experiment. Top panel: macroscopic stress versus macroscopic strain (black curve) and corresponding percentage of overcritical elements (blue curve). Bottom panels: Order of magnitude (logarithm in base 10) of the shearing deformation rate at the five stages indicated on the stress-strain plot.

In brief, these first experiments highlight important properties of the deformation simulated by the model:

1. the deformation is highly localized in space, i.e., heterogeneous (Marsan et al., 2004),
2. the deformation is strongly anisotropic, i.e. concentrates along linear kinematic features (Kwok 2001),
3. the deformation is localized in time, i.e, intermittent (Rampal et al., 2008).

As the applied strain increment is homogeneous in both space and time, these characteristics are not attributable to the external forcing but solely to the mechanics represented in the model.

Conclusion

First idealized experiments showed that the Maxwell-EB model is able to reproduce (1) the strong localization of deformation in both space and time, indicative of its heterogeneity and intermittency, (2) the natural emergence of the anisotropy of the deformation from an isotropic rheology (3) the asymmetry between successive periods of rapid damaging and slower recovery, (4) the persistence of activated leads (Coon et al., 2007) (5) the activation of new leads with different shapes and orientations, in agreement with the observed properties of the deformation of sea ice.

Sensitivity analyses and quantitative comparisons against Arctic buoy drift and RGPS deformation data are the next step in the development of the Maxwell-EB model. Such validation work necessitates carrying numerical experiments on realistic regional to global domains, over periods of days and longer. At these scales, deformations of the ice pack are large hence advection cannot be neglected. Unlike former, classical sea ice rheologies, the Maxwell-EB rheology effectively reproduces the very strong spatial gradients within the velocity, strain and stress fields of sea ice. This performance therefore requires the implementation of a robust advection scheme in order to limit diffusion and conserve the localization of the damage and deformation rates. The development of such an advection scheme is underway.

Acknowledgements

The financial support of TOTAL EP RECHERCHE DEVELOPPEMENT is gratefully acknowledged. V. Dansereau is supported by the Association National Recherche Technologie. She acknowledges support from the National Sciences and Engineering Research Council of Canada and the Fonds Québécois de la Recherche sur la Nature et les Technologies in the course of her Ph.D. A. Audibert-Hayet and K. Riska are thanked for valuable support and suggestions on this work.

References

Bouillon, S., J. Weiss, L. Girard, T. Fichevet, V. Legat and D. Amitrano: A further step towards the integration of the elasto-brittle rheology in sea ice models. Unpublished manuscript.

Byerlee, J., 1978: Friction of rocks. Pure and Applied Geophysics, 116(4-5), 615–626.

Coon, M. D., R. Kwok, G. Levy, M. Puis, H. Schreyer and D. Sulsky, 2007: Arctic Ice Dynamics Joint Experiment (AIDJEX) assumptions revisited and found inadequate. Journal of Geophysical Research, 112(C11S90), doi:10.1029/2005JC003393.

Girard, L., J. Weiss, J. M. Molines, B. Barnier, and S. Bouillon, 2009: Evaluation of high-resolution sea ice models on the basis of statistical and scaling properties of Arctic sea ice drift and deformation, Journal of Geophysical Research, 114, C08015, doi :10.1029/2008JC005182.

Girard, L., S. Bouillon, J. Weiss, D. Amitrano, T. Fichefet and V. Legat, 2011: A new modeling framework for sea-ice mechanics based on elasto-brittle rheology. Annals of Glaciology, 52(57), 123-132.

Hibler, W. D., III., 1977: A viscous sea ice law as a stochastic average of plasticity. Journal of Geophysical Research, 82, 3932 – 3938.

Hibler, W. D., III., 1979: A dynamic thermodynamic sea ice model. Journal of Physical Oceanogragphy, 9(7), 815–846.

Jaeger, J. C., and N. G. W. Cook, 1979: Fundamentals of rock mechanics. 593 pp.

Jop, P., Y. Forterre, and O. Pouliquen, 2006: A constitutive law for dense granular flows, Nature, 441, 727-730, doi:10.1038/nature04801.

Kenemy, J. and N. G. W. Cook, 1986: Effective moduli, Non-linear deformation and strength of a cracked elastic solid, International Journal of Rock Mechanics and Mining Sciences & Geomechanics Abstracts, 23(2), 107-118.

Kwok, R., 2001: Deformation of the arctic ocean sea ice cover between november 1996 and april 1997: a survey, Proceedings of the IUTAM Symposium on Scaling Laws in Ice Mechanics and Ice Dynamics, Fairbanks, Alaska, 315-322.

Marsan, D., H. Stern, R. Lindsay and J. Weiss, 2004: Scale dependence and localization of the deformation of arctic sea ice. Physical Review Letters, 93(178501).

Marsan D., J. Weiss, J.-P. Métaxian, J. Grangeon, P.-F. Roux, and J. Haapala, 2011: Low frequency bursts of horizontally-polarized waves in the Arctic sea-ice cover. Journal of Glaciology, 57(202), 231–237.

Petrich, C., P. Langhorne, and T. Haskell, 2007: Formation and structure of refrozen cracks in land-fast first-year sea ice, Journal of Geophysical Research, 112 (C4), C04,006.

Rampal, P., J. Weiss, D. Marsan, R. Lindsay, and H. Stern, 2008: Scaling properties of sea ice deformation from buoy dispersion analysis. Journal of Geophysical Research, 113(C03002), doi:10.1029/2007JC004143.

Sakov, P., F. Counillon, L. Bertino, K.A. Lisaeter, P. R. Oke and A. Korablev, 2012: TOPAZ4: an ocean-sea ice data assimilation system for the North Atlantic and Arctic. Ocean Sciences, 8, 633-656, doi:10.5194/os-8-633-2012.

Saramito, P., 2013: Efficient advanced scientific computing with Rheolef, CNRS-CCSD ed. http://cel.archives-ouvertes.fr/cel-00573970

Scholz, C.H., 2002: The Mechanics of Earthquakes and Faulting, Cambridge University Press, Cambridge, 471 pp.

Smith G. C., F. Roy, M. Rezka, M. Surcel, D. Colan, Z. He, D. Deacu, J.-M. Bélanger, S. Skachko, Y. Liu, F. Dupont, J.-F. Lemieux, C. Beaudoin, B. Tranchant, M. Drévillon, G. Garric, C.-E. Testut, J.-M. Lellouche, P. Pellerin, H. Ritchie, Y. Lu, F. Davidson, M. Buehner, A. Caya, M. Lajoie, 2014: Sea ice forecast verification in the Canadian Global Ice Ocean Prediction System. Submitted to the Quarterly Journal of the Royal Meteorological Society.

Weiss, J., E. M. Schulson, and H. L. Stern, 2007: Sea ice rheology from in-situ, satellite and laboratory observations: Fracture and friction. Earth and Planetary Science Letters, 255, 1–8.

Weiss, J. and E.M. Schulson. 2009: Coulombic faulting from the grain scale to the geophysical scale: lessons from ice. Journal of Physics D, 42(21), 214017, doi:10.1088/0022-3727/42/21/214017.